

UNCLASSIFIED

Copy
RM L9J27

NACA RM L9J27



NACA

RESEARCH MEMORANDUM

MEASUREMENTS OF THE DRAG AND PRESSURE DISTRIBUTION
ON A BODY OF REVOLUTION THROUGHOUT TRANSITION
FROM SUBSONIC TO SUPERSONIC SPEEDS

By Jim Rogers Thompson
Langley Aeronautical Laboratory
Langley Air Force Base, Va.

CLASSIFICATION CANCELLED

CLASSIFIED DOCUMENT

NOEAR 7 2479

Date 8/23/87

This document contains classified information
under Executive Order 11652 of the United
States within the meaning of the Espionage Act,
USC 50-31 and 32. Its transmission or the
revelation of its contents in any manner to an
unauthorized person is prohibited by law.
Information so classified may be imparted
only to persons in the military and naval
services of the United States, appropriate
civilian officers and employees of the Federal
Government who have a legitimate interest
therein, and to United States citizens of known
loyalty and discretion who of necessity must be
informed thereof.

NOA 9/7/54

See

NATIONAL ADVISORY COMMITTEE FOR AERONAUTICS

WASHINGTON

January 16, 1950

UNCLASSIFIED

UNCLASSIFIED

UNCLASSIFIED

NATIONAL ADVISORY COMMITTEE FOR AERONAUTICS

RESEARCH MEMORANDUM

MEASUREMENTS OF THE DRAG AND PRESSURE DISTRIBUTION
ON A BODY OF REVOLUTION THROUGHOUT TRANSITION
FROM SUBSONIC TO SUPERSONIC SPEEDS

By Jim Rogers Thompson

SUMMARY

As part of the general investigation by the National Advisory Committee for Aeronautics of the aerodynamic characteristics of promising airplane configurations and their component parts at transonic and supersonic speeds, the drag and pressure distribution on a body of revolution of fineness ratio 12 have been measured by the free-fall method. Results are presented for Mach numbers from 0.75 to 1.27 and are the first complete measurements obtained at large scale under actual flight conditions of the pressure distribution on a body of revolution at zero angle of attack throughout the transition from subcritical to moderate supersonic speeds.

Analysis of the results obtained has provided knowledge of the mechanism of the abrupt drag rise which occurs near the speed of sound, and has demonstrated that the theoretical method of NACA TN 1768 satisfactorily predicts the shape of the measured pressure distributions at low supersonic speeds. Limited information on the skin-friction drag of the body is also presented.

INTRODUCTION

As part of the general investigation by the NACA of the aerodynamic characteristics of promising airplane configurations and their component parts at transonic and supersonic speeds, the drag and pressure distributions on a body of revolution of fineness ratio 12 have been measured by the free-fall method. The object of this measurement was twofold: To provide understanding of the character of the flow in order to facilitate the development of means for minimizing the abrupt drag rise near the speed of sound; and to provide experimental confirmation of the

UNCLASSIFIED

method presented in reference 1 for computing the pressure distribution at supersonic speeds on a slender, arbitrary body of revolution.

The shape of the body tested was designed in 1944 at the inception of the free-fall test program in an attempt to provide a basic body shape which had the highest possible critical speed. It was felt that a high critical speed would be one of the salient features of a body having desirable transonic and supersonic drag characteristics. The basic body shape has its maximum diameter located at the body midpoint and, in comparison with a parabola, is more blunt at the nose and less blunt at the tail. The rear part of the basic body shape is cusped; however, as used in the free-fall tests, a boom supporting the stabilizing tail surfaces is faired into the rear of the body covering part of the cusp.

Bodies of this basic shape having a fineness ratio of 12 have been used as a standard body in the free-fall tests of wing-body combinations presented in reference 2 and in other papers. The transonic and supersonic drag characteristics of the body-tail combination without wings were presented in reference 3.

The results presented herein are the first complete measurements obtained at large scale under actual flight conditions of the pressure distribution on a body of revolution at zero angle of attack throughout the transition from subcritical to moderate supersonic speeds.

Curves showing the variations with Mach number of significant drag and pressure parameters measured between $M = 0.75$ and 1.27 are presented and discussed.

METHOD

The test was performed by utilizing the free-fall method (described in references 2 and 3) in which the flight path of the freely falling test body is obtained by radar and phototheodolite equipment and other required quantities are measured at the body by means of the NACA radio-telemeter system.

Model.- A drawing showing details and dimensions of the test model is presented as figure 1, and photographs showing the complete model and details of the nose and the body-tail boom junction are presented as figure 2. The coordinates of the body surface are given in table I. The external shape of the model was the same as that of the body-tail combinations of the wing-body combinations treated in reference 2 and differed from that of reference 3 only by the addition of the airspeed boom. The model was constructed entirely of metal and weighed 586.5 pounds.

Measurements.- In addition to the usual measurements of velocity, flight path, over-all drag (retardation), tail drag, and total and static pressures at the airspeed head (see reference 2), the pressures at 19 flush orifices on the body surface were measured by differential-pressure cells. The location of the orifices (expressed as a fraction of the body length, x/l) and the numbers by which they are identified hereinafter are shown in figure 1 and are tabulated in table II. The pressure at orifice 19 (near the front of the tail boom) was measured with respect to the static pressure at the airspeed head, and the pressures at the remaining orifices were measured with respect to the pressure at orifice 19. This arrangement was chosen to retain the advantages of the small-range differential-pressure cells without incurring excessive lag due to the necessarily small size of the static holes in the airspeed head. Orifice 19 (see fig. 2(c)) was made large enough so that the computed lag was less than 0.01 second. The indication from each pressure cell was sampled at least three times per second (corresponding to a minimum of 2 points per 0.01 change in Mach number) by means of electrical switching equipment.

Precision of measurements.- Previous experience has shown that the possible inaccuracy of a telemetered measurement is of the order of ± 1 percent of the full range of the instrument and that the maximum possible error in the Mach number determined from the flight-path measurements (combined with wind and temperature data) is less than ± 0.01 . Based on these values, the maximum inaccuracies of the drag parameters determined from acceleration and force measurements (drag coefficients C_{DF} are based on body frontal area and drag per unit of body frontal area expressed as a fraction of static pressure D/F_p) are as follows:

Drag parameter		Mach number			
		0.75	0.95	1.05	1.25
D/F_p	Total	± 0.004	± 0.003	± 0.002	± 0.002
	Tail	± 0.003	± 0.002	± 0.002	± 0.001
	Body	± 0.007	± 0.005	± 0.004	± 0.003
C_{DF}	Total	± 0.012	± 0.008	± 0.007	± 0.006
	Tail	± 0.009	± 0.005	± 0.004	± 0.002
	Body	± 0.020	± 0.010	± 0.008	± 0.006

The inaccuracy in the indication of a single-range instrument decreases appreciably with increase in Mach number, as both the speed and static pressure (and therefore the ratio of the measured value to the full-scale value) increase rapidly during the free fall of the model. A multiple accelerometer having three ranges was incorporated in the subject model. This accelerometer enabled more accurate measurements of the low values of acceleration which occurred during the early part of the drop to be made so that the possible inaccuracy in total drag at low Mach numbers was considerably less than that obtained in reference 3. The inaccuracy presented for the body-drag parameters were based on the sum of the possible drag inaccuracies of the total- and tail-drag measurements as the body drag was computed by subtracting the measured tail drag from the measured total drag. The most probable value of the inaccuracy in the body-drag parameters is of course smaller than the value presented. The values in the table for the maximum inaccuracy in the body-drag coefficient C_{DF} are slightly less than the sum of the total and tail inaccuracies because the maximum error in the Mach number (0.01) enters only once in each computation.

The estimated maximum inaccuracy in the pressure coefficient P as obtained from the differential cells decreases from about ± 0.04 at $M = 0.75$ to ± 0.02 at $M = 0.95$ and to ± 0.004 at a Mach number of 1.27.

RESULTS

The accuracy of the total drag obtained from the retardation measurements is confirmed by the excellent agreement of the variations with time of the velocity and altitude obtained by integration of the vector sums of the measured and gravitational accelerations with the corresponding variations obtained from the radar and phototheodolite equipment. The variation of Mach number with time used herein was computed from the velocity data just described by use of atmospheric wind and temperature data. The accuracy of this Mach number near sonic speeds is confirmed by the results of an investigation of nose-mounted airspeed installations presented in reference 4. The results of reference 4 predict that passage of the body bow wave over the static orifices of the airspeed head should have occurred between Mach numbers 1.000 and 1.003 during the present test, provided that the body nose was parabolic. Although the nose of the test body is not parabolic, the differences are small and would not significantly change the Mach number for bow-wave passage. Good agreement was obtained between these predicted results and the test results as the static pressure at the airspeed head showed an abrupt drop of the correct order of magnitude

beginning at a Mach number of 1.005. The Mach number determined by the other methods is within the estimated possible inaccuracy of the absolute-pressure measurements. The static-pressure error of the air-speed head was obtained by correlation of the telemetered pressure with atmospheric pressure at the same radar altitude, and the maximum errors in static-pressure coefficient were about 0.02 near $M = 1.00$ and -0.01 above $M = 1.20$. These errors are within the estimated possible inaccuracy of the telemetered pressures (due to the necessarily large range of the instruments) and are therefore not significant.

The basic measurements made during the free fall of the model are presented in figures 3 and 4 and have been reduced to coefficient form through use of the variation of atmospheric pressure and temperature with altitude. These measurements were made immediately following the test.

Drag measurements.- Figure 3 presents the variation with Mach number of the drag per unit of body frontal area as a fraction of atmospheric pressure (D/F_p) and of the drag coefficient based on body frontal area C_{D_F} as obtained from the total-drag (retardation) and tail-drag measurements. The division of the total drag between the body and the stabilizing tail surfaces is also shown. The abrupt drag rise of the tail surfaces began at a Mach number of 0.90 and continued until a Mach number of 0.97 was reached. From $M = 0.97$ to the highest Mach number reached by the model ($M = 1.27$), the increment of drag coefficient chargeable to the tail decreased slightly. The drag coefficient of the body had no significant variations up to a Mach number of about 0.995 where it increased abruptly until a Mach number of 1.01 was reached. The drag coefficient of the body increased slightly as the Mach number increased beyond 1.01.

Pressure measurements.- The variation with Mach number of the pressure coefficient P at each orifice is presented in figure 4. The discrepancies between the theoretical curves (also included in fig. 4) and the experimental data are discussed subsequently.

Because of the extremely small magnitude of the pressure differences occurring at low Mach numbers and high altitude, the possible inaccuracies in P are large (see "Precision of measurements") and therefore data are not presented for Mach numbers lower than 0.75. Immediately after release, oscillations, which were usually within the estimated error, were evident in the pressure records. For most of the orifices, these oscillations damped rapidly and disappeared within a few seconds after the release of the model. In two cases (orifices 17 and 18), however, the oscillations were large and, although they decreased in amplitude with time, they did not disappear until Mach numbers of about 1.00 and 0.80 were reached for orifices 17 and 18, respectively.

A dashed fairing is presented in figure 4 in the region when this oscillation occurred. No plausible explanation of the oscillation has been advanced, although it should be noted that orifices 17 and 18 are located on the circular-arc fairing between the body and the tail boom where theory indicates that a very steep peak in the pressure distribution should occur.

As the difference between the true static pressure and the static pressure measured at the airspeed head was small and less than the inaccuracy of the measurement (discussed previously), no correction for the static-pressure error of the airspeed head has been applied to the pressure-coefficient data presented herein. Reference 4 indicates that the static error should be negligible for the subject body-airspeed boom configuration.

The indicated pressure for orifice 3 became increasingly negative during the drop, approximately following the inverse of the static-pressure variation. As this is the type of variation which would occur if the tube were pinched or plugged, it is considered probable that tube 3 was damaged during the final assembly of the model. For this reason, data for orifice 3 are not presented herein.

DISCUSSION

Pressure Data

In order to provide an over-all picture of the flow about the body throughout the investigated Mach number range, the basic data of figure 4 are plotted in figure 5 as the variation of local Mach number along the body surface for values of free-stream Mach number between 0.84 and 1.26 in increments of 0.02. The most notable feature shown by figure 5 is the marked similarity of all subsonic distributions and the corresponding marked similarity of all the supersonic distributions; the transition phenomena associated with the drag rise appear to occur almost entirely between Mach numbers of 0.98 and 1.02. It is evident that there is little change in the character of the flow at the nose of the body during the transition through the speed of sound. The major changes are the gradual steepening of the approximately linear variation of local Mach number along the middle part of the body as the critical Mach number is exceeded and the abrupt increase in the rearward extent of this approximately linear region which occurs at the speed of sound.

For detailed study of the flow over the body, the basic data of figure 4 are cross-plotted in figure 6 in the form of pressure coefficient P against orifice location x/l for several Mach numbers.

In each case, the measured distributions are compared with the theoretical results. The distributions for each speed range are discussed separately.

Subcritical speeds.- In figures 6(a), 6(b), and 6(c), the measured distributions for $M = 0.75$, 0.90 , and 0.95 are compared with theoretical distributions computed for $M = 0$ by approximate linearized methods and corrected to the appropriate Mach number by application of the Prandtl-Glauert rule for slender bodies of revolution (reference 5). In general, the agreement is quite satisfactory except at the extreme rear of the body where the experimental data are subject to some doubt due to the oscillations discussed in "RESULTS" and where the approximate theory could hardly be expected to indicate accurately the large and abrupt variations which occur near the fairing between the body and the tail boom ($\frac{x}{l} = 0.9$ to 0.94). In view of the large pressure recovery measured on the rear of the body, it is considered unlikely that any appreciable flow separation occurred. The theoretical correction for the effect of Mach number appears to be in fair agreement with the measured increase in pressure coefficient with increase in Mach number. This agreement is shown more clearly in the subcritical part of figure 4 and confirms similar results presented in figure 6. Of course, the method of reference 5 is strictly applicable only at the maximum diameter of an elliptical body, but figure 4 shows that the agreement is about as satisfactory at most points of the subject body, excluding the extreme nose and tail, as at the maximum diameter.

With the exception of orifice 7 ($\frac{x}{l} = 0.392$), the measured points are consistent within considerably less than the estimated maximum uncertainty given in "Precision of measurements." The pressure at this orifice was greater than that at either orifice 6 or 8 at both subsonic and supersonic speeds although such a tendency was not evident in the theoretical distributions for either speed range. Since the values at orifice 7 fair smoothly with those farther to the rear at Mach numbers above 0.90 , it is possible that the fairing of the body near and immediately behind the construction joint in the body between orifices 6 and 7 differed slightly from that specified. The theoretical calculations were based on the specified fairing.

Supersonic speeds.- The measured pressure distributions at several supersonic Mach numbers are compared in figures 6(g) to 6(k) with results computed by the method of reference 1. Except for the "bump" at orifice 7 (mentioned in "Subcritical speeds") it is evident that the shapes of the measured and computed distributions are nearly identical even in the region of abrupt pressure recovery at the tail of the model. Examination of the supersonic part of figure 4 shows that the theory

also gives the trend of pressure coefficient with Mach number for each orifice within reasonable limits. It is evident from the figures, however, that the level of the measured distributions is consistently more positive than that of the theoretical distributions. The level of the measured distributions results in a drag of the forward part of the body which is larger than the drag of the rear part of the body at low supersonic speeds. This division of drag is opposite to results obtained from wing-flow tests of a parabolic body of fineness ratio 6. (See reference 7.) In view of this discrepancy, the experimental level is subject to question unless confirmed by later measurements.

Several possible causes of the high level have been investigated and it is considered probable that the effect resulted from incorrect measurement of the pressure difference between orifice 19 and the static head. As the pressures at orifices 1 to 18 were measured with respect to the pressure at 19 and referred to static pressure by use of the indication of cell 19 (see "Measurements"), an error of a particular type would have had to be present to give the observed result. It was found that an error of about the correct order of magnitude and variation would result if a restriction were present in the tube between the static head and cell 19 which almost closed off the tube. The error resulting from such a restriction would be greater at supersonic speeds than at subsonic speeds because of the increasing rate of change of static pressure throughout the drop. Since the existence of the restriction cannot be verified, confirmation of the theoretical level must await further measurements.

The shape of the measured distributions shown in figures 6(g) to 6(k) is more linear than the theoretical distributions near the nose. In the theoretical computations, the body was assumed to be sharp-pointed, the rapidly decreasing pressure behind the nose resulting from the relatively abrupt curvature in this region. The test body, however, was fitted with an airspeed boom, which, though small, would cause changes of the type observed by masking the assumed sharp point and part of the abrupt curvature. The presence of the airspeed boom also affects the shock-attachment phenomena at the nose of the body. The angle between the boom and the body at the intersection is about 15° . If the attachment occurred as on a sharp-pointed cone, the shock would stand at the intersection for all Mach numbers above about 1.10, and the flow over the entire forward part of the body would be supersonic. The experimental data in figure 6, however, show that the local velocity at orifice 1 (immediately behind the nose) is appreciably subsonic at $M = 1.10$ and it is evident that the flow is not exactly conical in this region.

It is of interest to note that the distribution computed by the method of reference 1 for $M = 1.05$ agrees with the measurements as satisfactorily as at the higher speeds, even though there is no attached

shock and large subsonic regions are present at the nose and tail of the body.

Transonic speeds.- Although some doubt exists as to the exact level of the pressure measurements at supersonic speeds, the data presented herein show the mechanism of the changes in flow which occur during the abrupt drag rise. Figure 5 provides an over-all view of the changes and figures 4 and 6 provide more detailed information. Measured pressure distributions at $M = 0.99$, 1.00 , and 1.01 are presented in figures 6(d) to 6(f). As no directly applicable theory exists, these data are compared with the theoretical distributions for $M = 0.95$ and 1.05 . Examination of figure 6(d) shows that at $M = 0.99$ the data agree with the subsonic theory about as satisfactorily as at $M = 0.95$ except between values of x/l from 0.6 to 0.7 where the data tend to follow the supersonic theory. At $M = 1.00$, the agreement is similar, differing only in that the region resembling the supersonic theory extends from about x/l of 0.5 to about 0.75 . At $M = 1.01$, however, the data for the rear of the body agree almost exactly with the supersonic theory. On the nose of the body there is very little change in the distribution between $M = 0.99$ and 1.01 . A tendency toward steepening the velocity variation which occurs near orifice 6 ($\frac{x}{l} = 0.3$) as the Mach number approaches unity might be taken as indicating that a small shock existed between orifices 6 and 7. If this shock did exist, it must have resulted from a small discontinuity on the body as examination of the data for orifice 7 in figure 4 shows that no shock passed over this orifice.

As the Mach number increases from a subsonic value, figure 5 shows that the pressure recovery behind the maximum velocity on the body ($\frac{x}{l} \approx 0.68$) gradually becomes more abrupt, and, as indicated by figure 4, a shock wave begins to form between orifices 11 and 12. This shock wave moves rearward with further increase in Mach number. (See fig. 4.) At $M = 0.997$ it passes over orifice 12 and, rapidly moving rearward, passes over orifice 13 at $M = 1.00$ and orifice 14 at about $M = 1.005$. After this orifice, however, the shock wave approaches the region where an abrupt compression would occur naturally because of the curvature of the body and body-tail boom juncture, and there is no further evidence of a shock on the body as the Mach number is further increased.

Apparently, as the local Mach number ahead of the region of "natural" compression approaches unity (or some critical value near unity), the effect of the region of compression on the velocities ahead of it is decreased, which causes the local velocities to increase still further. This obviously unstable phenomenon rapidly grows into a shock wave which moves back along the body and increases in strength until possibly it is forced away from the body by the natural compression. It appears

reasonable to assume that the shock exists in space away from the body as the coalescence of infinitely small compression waves which make up the natural compression on the rear of the body at supersonic speeds. Confirming evidence of such a shock standing away from the body by as much as 1 body diameter has been obtained from shadowgraph pictures of the flow about a body-tail boom combination of fineness ratio 6 in a 12-inch-square wind tunnel at a Mach number of 1.5.

Drag Data

The direct measurements of the total and the tail drag presented previously (fig. 3) allow the body drag to be computed, and, as the body pressure drag may be obtained by integration of the measured pressure distributions, the variations with Mach number of the skin-friction drag may be derived. The drag characteristics of each component of the subject model throughout the investigated speed range and the mechanism of the abrupt rise which occurs in the body drag near the speed of sound are compared with appropriate theory and measurements and are discussed in the following paragraphs.

Drag of the complete model.- The variation with Mach number of the drag coefficient for the complete model as obtained from the longitudinal accelerometer (fig. 3) is reproduced in figure 7 where it is compared with similar data taken from reference 3. As discussed in "Precision of measurements," the drag measurement for the subject model was several times more accurate than that of reference 3 at subsonic and transonic speeds. Thus, the tail drag rise which occurs at $M = 0.90$ is seen to be completed at $M = 0.97$ and the body drag rise does not begin until a Mach number of about 1.00 is reached. These detail variations were not apparent in the tests of reference 3 because of the lower sensitivity of the accelerometers then available. Near $M = 1.10$ where the value of the drag is appreciable, satisfactory agreement is obtained. At higher Mach numbers, however, the curves diverge; data from the subject test continue to increase slightly, while the data from reference 3 decrease with increase in Mach number. The discrepancy at $M = 1.27$ is greater than the sum of the estimated maximum inaccuracies of both measurements. It should be noted that the data from reference 3 are a fairing of results of three bodies, and, although they showed slight differences in magnitude, all decreased with increase in Mach number at about the same rate. The models differed only in that the subject model had an airspeed boom while the models of reference 3 did not. Further research, particularly on skin-friction phenomena at transonic speeds, may provide a satisfactory explanation of the discrepancy.

Drag of the tail.- The variation with Mach number of the tail drag coefficient (based on body frontal area) is presented in the lower part

of figure 7 where it is compared with a band taken from reference 2 which includes data from several identical tails measured on other free-fall test bodies. It is evident that the tail-drag data for the subject model agree satisfactorily with the previous measurements.

Drag of the body.- The variation with Mach number of the body-drag coefficient computed from the difference between the measured drags of the complete model and of the tail is presented in figure 8. The accuracy of the basic measurements is indicated by the absence of any large fluctuations in the experimental body-drag curve between $M = 0.9$ and $M = 1.0$. In this region, the drag of the tail increases rapidly. After the abrupt drag rise of the tail, but before that of the body, the drags of the body and tail are of the same order of magnitude, whereas below $M = 0.90$ and above $M = 1.00$ the tail drag was considerably smaller than that of the body. It is evident from figure 8 that the abrupt drag rise of the body starts at $M = 0.995$ and is completed by $M = 1.015$. Above this Mach number, the body-drag coefficient continues to rise at a decreasing rate.

Body pressure drags.- The measured pressure distributions were integrated to find the body-pressure-drag coefficient based on body frontal area CD_{FP} and the values obtained are presented in figure 8 for comparison with the body drag previously determined. It is evident that the shapes of the body-drag and body-pressure-drag variations with Mach number are nearly identical. As the integration is closed except for the area of the tail boom, the values of CD_{FP} are not sensibly affected by the possible inaccuracy in the level of the supersonic distributions but are determined by the shape of the distributions. The area of the tail boom is only 4 percent of the frontal area of the body and it is estimated that the possible inaccuracy in CD_{FP} resulting from the neglect of the pressure-level error times this area is of the order of 0.002, which is about one-half the estimated maximum error due to the fairing of the distributions between orifices. The values of CD_{FP} are nearly zero until the abrupt drag rise starts at $M = 0.995$.

The pressure-drag coefficient computed for the subject body by the theoretical method of reference 1 is also presented in figure 8. This theoretical value, which is independent of Mach number, has a value of 0.08 and is considered to be in satisfactory agreement with the experimental data above the Mach number of 1.05.

Although the possible inaccuracy in the level of the supersonic pressure distribution necessarily precludes reliable determination of the actual values of the pressure drag of the front and of the rear of the body, there are certain features of the measured variations of these component drags worth noting. It was found that the drag coefficient of the rear part of the body remained almost constant up to $M = 0.995$ and

then increased abruptly between $M = 0.995$ and 1.01 , followed by a relatively small decrease between $M = 1.01$ and 1.03 . No significant variations were apparent at higher Mach numbers. The drag coefficient of the forward part of the body remained almost constant up to $M = 1.005$ and then increased rapidly between $M = 1.005$ and 1.025 . The rate of increase gradually became less as the Mach number further increased and no significant variations in drag coefficient occurred at Mach numbers greater than 1.05 .

Mechanism of the drag rise.- The drag data presented in the preceding paragraphs, together with the pressure data, provide a complete description of the mechanism of the abrupt rise in the drag of a body of revolution during its passage through the speed of sound. It is evident that as the Mach number is increased above the critical value, the supersonic region grows (the pressure distribution within the region resembling part of a supersonic distribution) without noticeable increase in either the pressure drag or the total drag of the body. As the speed of sound is approached, however, a point is reached where the supersonic region has grown to the extent that a shock of finite strength forms at the rear of the region. The presence of this shock causes the supersonic region to grow still more and the shock rapidly becomes stronger and moves downstream. The abrupt rise in the pressure drag and total drag of the rear of the body is directly associated with the rearward movement of the shock. As the speed of sound is exceeded, the drag of the forward part of the body begins to rise at a rate considerably slower than the drag rise of the rear part of the body. The pressures on the nose gradually change in a positive direction without appreciably altering the shape of the distribution, and the drag appears to approach its supersonic value asymptotically as the subsonic region at the nose becomes negligible. The decrease in the pressure drag of the rear of the body which follows the abrupt rise is believed to result from a readjustment of the flow over the rear of the body due to the increasing amount of supersonic flow over the nose.

The present results confirm the preliminary description of the mechanism of the drag rise which was first deduced from measurements of the over-all drag of bodies having different locations of the maximum diameter (reference 8). Further confirmation is obtained from the small-scale pressure-distribution measurements presented in references 6 and 7.

Body skin-friction drag.- The variation with Mach number of the skin-friction drag coefficient determined as the differences between the two experimental curves of figure 8 is presented in figure 9. Although the inaccuracy of the values determined in this way is necessarily large, particularly at the lower Mach numbers, it is evident that the skin-friction drag coefficient does not vary appreciably with Mach number. The experimental values of skin-friction drag

coefficient are compared in figure 9 with theoretical values calculated by the method of Young, reference 9, for the cases of transition at the nose and transition at the body midpoint. The variation of Reynolds number throughout the free fall of the model on which the theoretical calculations were based is presented in figure 10. Good agreement is obtained between the theoretical result for transition at the nose and the experimental data up to a Mach number slightly exceeding 1.0. Beyond this value, the experimentally determined skin friction is somewhat higher than the theoretical value. Explanation of the discrepancies evident in these preliminary data must await more complete understanding of skin-friction and transition phenomena at transonic and supersonic speeds.

An additional point to be considered in the analysis of the skin friction on the body is the low temperature of the body surface. Although the insulated instrument compartment is heated, the surface temperature at release is probably very close to the free-air temperature. As the heat capacity of the cast-iron body is large, the surface temperature of the body will not increase appreciably during the 50 seconds of the free fall. The atmospheric conditions measured at the release and impact of the subject model are shown in figure 10, and if the surface temperature throughout the fall remains at approximately the free air temperature at the release altitude, the surface temperature at impact would be about 145° F lower than the local atmospheric temperature. Heat-flow effects are, of course, not considered in reference 9 but other theoretical analyses have indicated that heat flow to the body should decrease the friction drag.

CONCLUSIONS

The drag and pressure distribution on a body of revolution of fineness ratio 12 have been measured between Mach numbers of 0.75 and 1.27 at large scale under actual flight conditions by the free-fall method. Analysis of the results obtained led to the following conclusions:

1. The mechanism of the abrupt rise in the drag of a body of revolution as the Mach number is increased through unity is described in four steps:

- (a) As the critical Mach number is exceeded, the supersonic region first grows with no attendant increase in drag coefficient.

(b) As the Mach number approaches unity, a shock is formed at the rear of the supersonic region. The shock rapidly moves rearward and the supersonic region rapidly expands. The abrupt drag rise on the rear of the body is directly associated with the rearward motion of the shock.

(c) As the Mach number exceeds unity, the pressures on the forward part of the body gradually change in a positive direction without appreciably altering the shape of the distribution, the drag coefficient increasing at a considerably smaller rate than that of the rear of the body.

(d) As the Mach number further increases, the rate of increase in drag coefficient of the forward part of the body gradually becomes less and no significant changes occur above a Mach number of 1.05. The drag coefficient of the rear part of the body shows a relatively small but abrupt decrease immediately after its abrupt rise and then has no significant changes with further increase in Mach number.

2. The theoretical method of NACA TN 1768 satisfactorily predicted the shape of the measured pressure distributions at low supersonic speeds even in the region of abrupt pressure recovery on the rear of the body and at a Mach number of 1.05 where a relatively large subsonic region existed at the nose. As a result of a possible inaccuracy in the level of the pressure measurements at supersonic speeds, the level of the distributions predicted by the method of NACA TN 1768 must await further experimental confirmation.

3. Although the values of skin friction obtained are subject to the uncertainties attendant to indirect measurement, it appears that the skin-friction drag coefficient on the subject body is nearly constant throughout the investigated Mach number range. It is considered that further study of friction drag at transonic speeds would be desirable.

Langley Aeronautical Laboratory
National Advisory Committee for Aeronautics
Langley Air Force Base, Va.

REFERENCES

1. Thompson, Jim Rogers: A Rapid Graphical Method for Computing the Pressure Distribution at Supersonic Speeds on a Slender Arbitrary Body of Revolution. NACA TN 1768, 1949.
2. Thompson, Jim Rogers, and Mathews, Charles W.: Effect of Wing Sweep, Taper, and Thickness Ratio on the Transonic Drag Characteristics of Wing-Body Combinations. NACA RM L8K01, 1948.
3. Thompson, Jim Rogers, and Mathews, Charles W.: Total Drag of a Body of Fineness Ratio 12 and Its Stabilizing Tail Surfaces Measured during Free Fall at Transonic Speeds. NACA CB L6D08, 1946.
4. Danforth, Edward C. B., and Johnston, J. Ford: Error in Airspeed Measurement Due to Static-Pressure Field ahead of Sharp-Nose Bodies of Revolution at Transonic Speeds. NACA RM L9C25, 1949.
5. Lees, Lester: A Discussion of the Application of the Prandtl-Glauert Method to Subsonic Compressible Flow over a Slender Body of Revolution. NACA TN 1127, 1946.
6. Danforth, Edward C. B., and Johnston, J. Ford: Pressure Distribution over a Sharp-Nose Body of Revolution at Transonic Speeds by the NACA Wing-Flow Method. NACA RM L7K12, 1948.
7. Johnston, J. Ford, and Lopatoff, Mitchell: Study by NACA Wing-Flow Method of Transonic Drag Characteristics of a Blunt-Nose Body of Revolution and Comparison with Results for a Sharp-Nose Body. NACA RM L9C11, 1949.
8. Thompson, Jim Rogers, and Kurbjun, Max C.: Drag Measurements at Transonic Speeds of Two Bodies of Fineness Ratio 9 with Different Locations of Maximum Body Diameter. NACA RM L8A28b, 1948.
9. Young, A. D.: The Calculation of the Total and Skin Friction Drags of Bodies of Revolution at Zero Incidence. R. & M. No. 1874, British A.R.C., 1939.

TABLE I
COORDINATES OF FINENESS-RATIO-12 BODY

[Nose radius, 0.060 in.]

X (in.)	Y (in.)	X (in.)	Y (in.)
0	0	48.00	4.876
.60	.277	54.00	4.971
.90	.358	60.00	5.000
1.50	.514	66.00	4.955
3.00	.866	72.00	4.828
6.00	1.446	78.00	4.610
9.00	1.936	84.00	4.274
12.00	2.365	90.00	3.754
18.00	3.112	96.00	3.031
24.00	3.708	102.00	2.222
30.00	4.158	108.00	1.350
36.00	4.489	114.00	.526
42.00	4.719	120.00	0

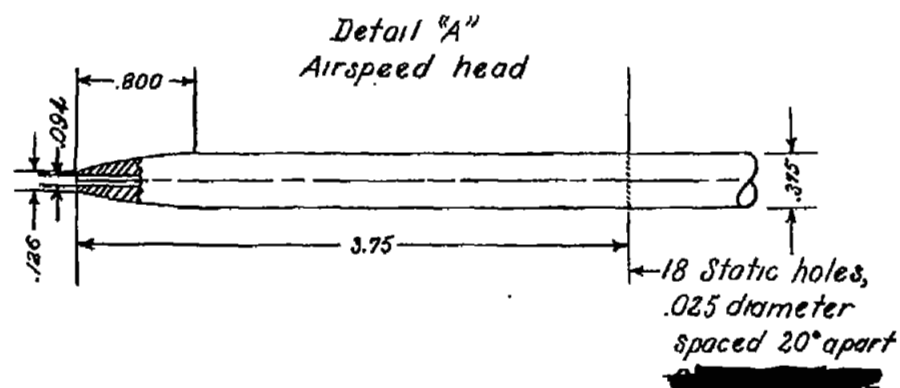
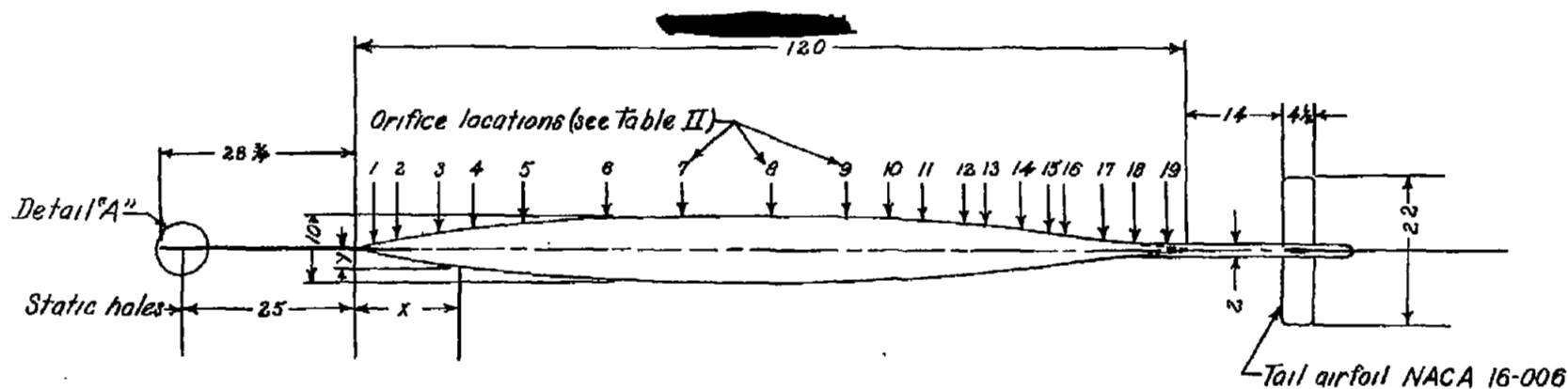
NACA

TABLE II
LOCATION OF ORIFICES ON BODY

Orifice (1)	Location on body	
	Distance from nose (in.)	Fraction of body length, x/l
1	2.50	0.021
2	6.00	.050
3	12.00	.100
4	17.00	.142
5	24.00	.200
6	36.00	.300
7	47.00	.392
8	60.00	.500
9	71.00	.591
10	77.00	.642
11	82.00	.683
12	88.00	.733
13	91.00	.758
14	96.00	.800
15	100.00	.833
16	102.30	.852
17	108.30	.902
18	112.50	.937
19	117.30	.977

¹Orifice diameter is 3/32 inch, excepting orifice 19 which consisted of six 3/16-inch holes connected to a common manifold.

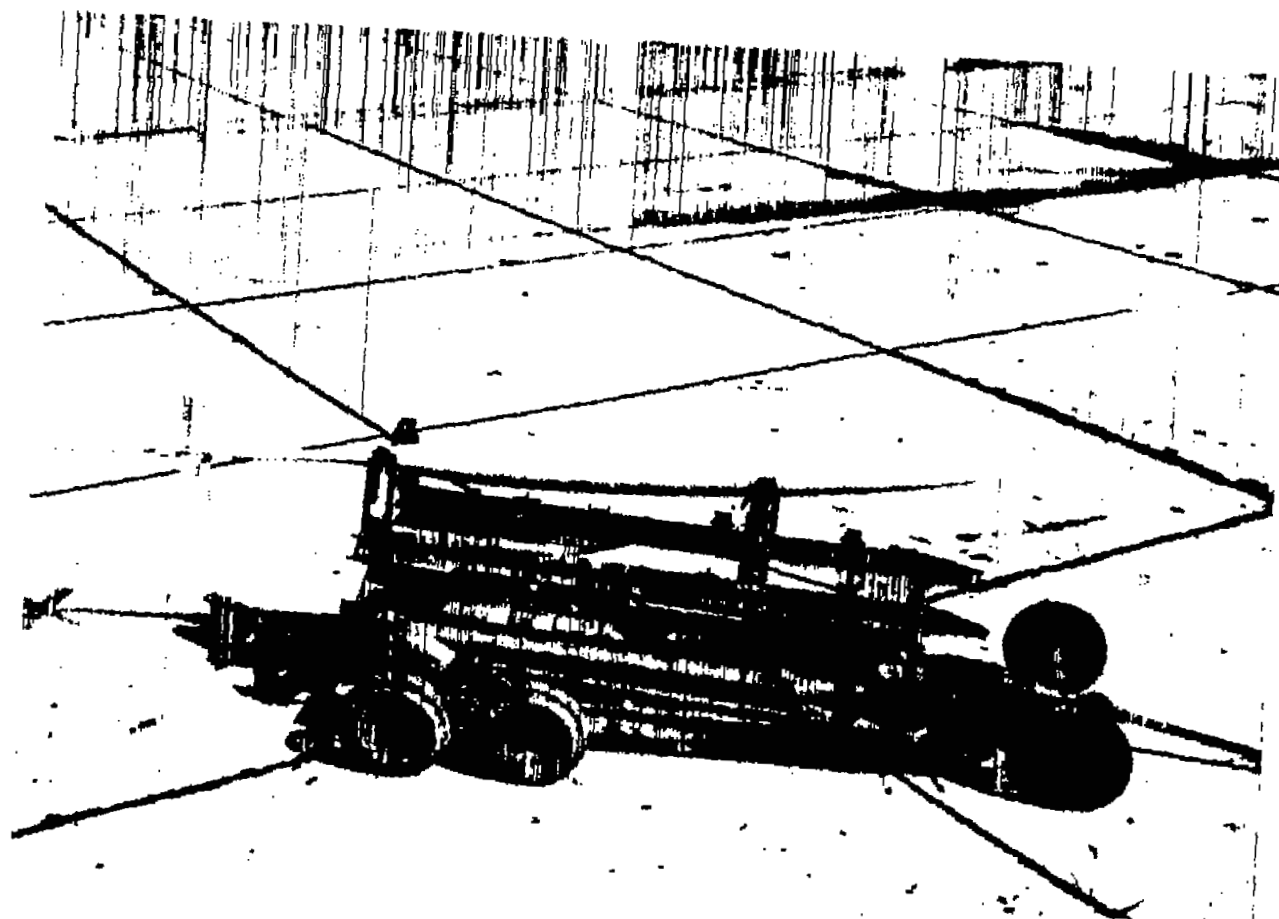
NACA



Dimensions	
Body frontal area, sq ft	0.545
Tail frontal area, sq ft	0.074
Total frontal area, sq ft	0.619
Surface area, sq ft (body)	17.990
Volume, cu ft (body)	3.080



Figure 1.- Details and dimensions of the complete model. The coordinates of the body surface are given in table I and orifice locations are given in table II. All dimensions are in inches.

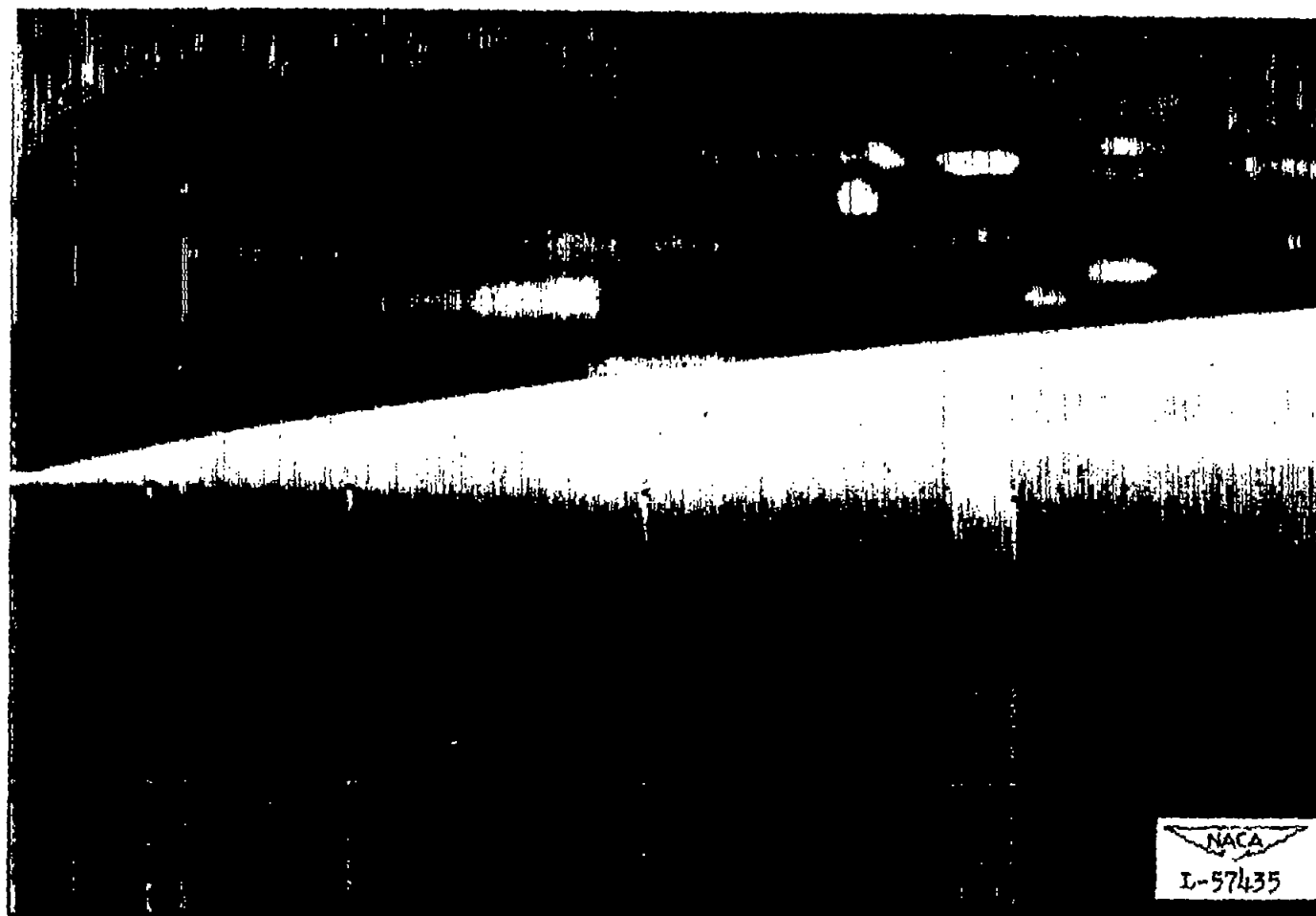


(a) Complete model.



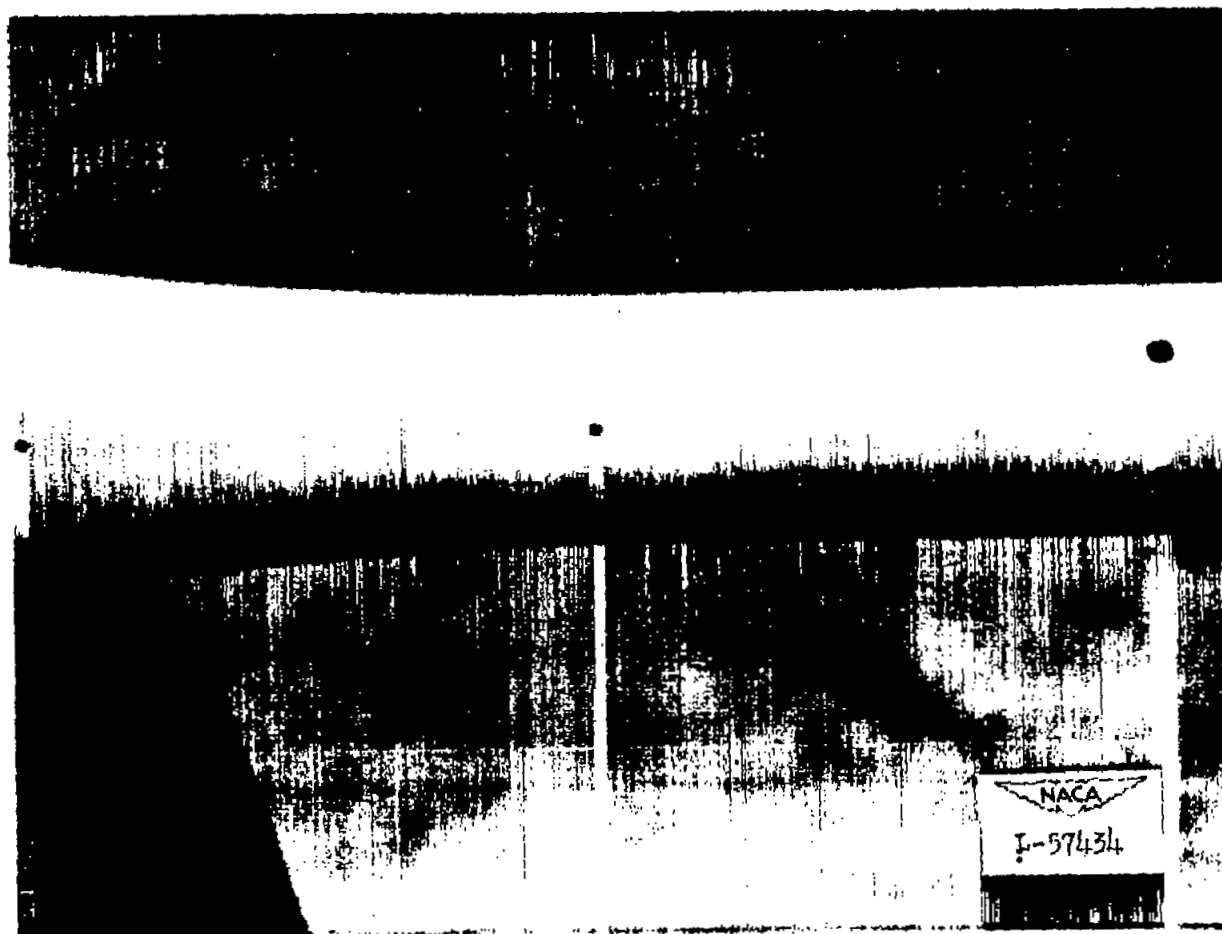
L-57435.1

Figure 2.- Photographs of model.



(b) Detail of nose showing body-airspeed-boom juncture and orifices 1 to 4.

Figure 2.- Continued.



- (c) Detail of rear part of body showing body-tail-boom juncture and orifices 17 to 19. Orifice 19 (to which the other pressures were referred) consisted of 6 large holes connected together inside the tail boom to minimize the lag.

Figure 2.- Concluded.

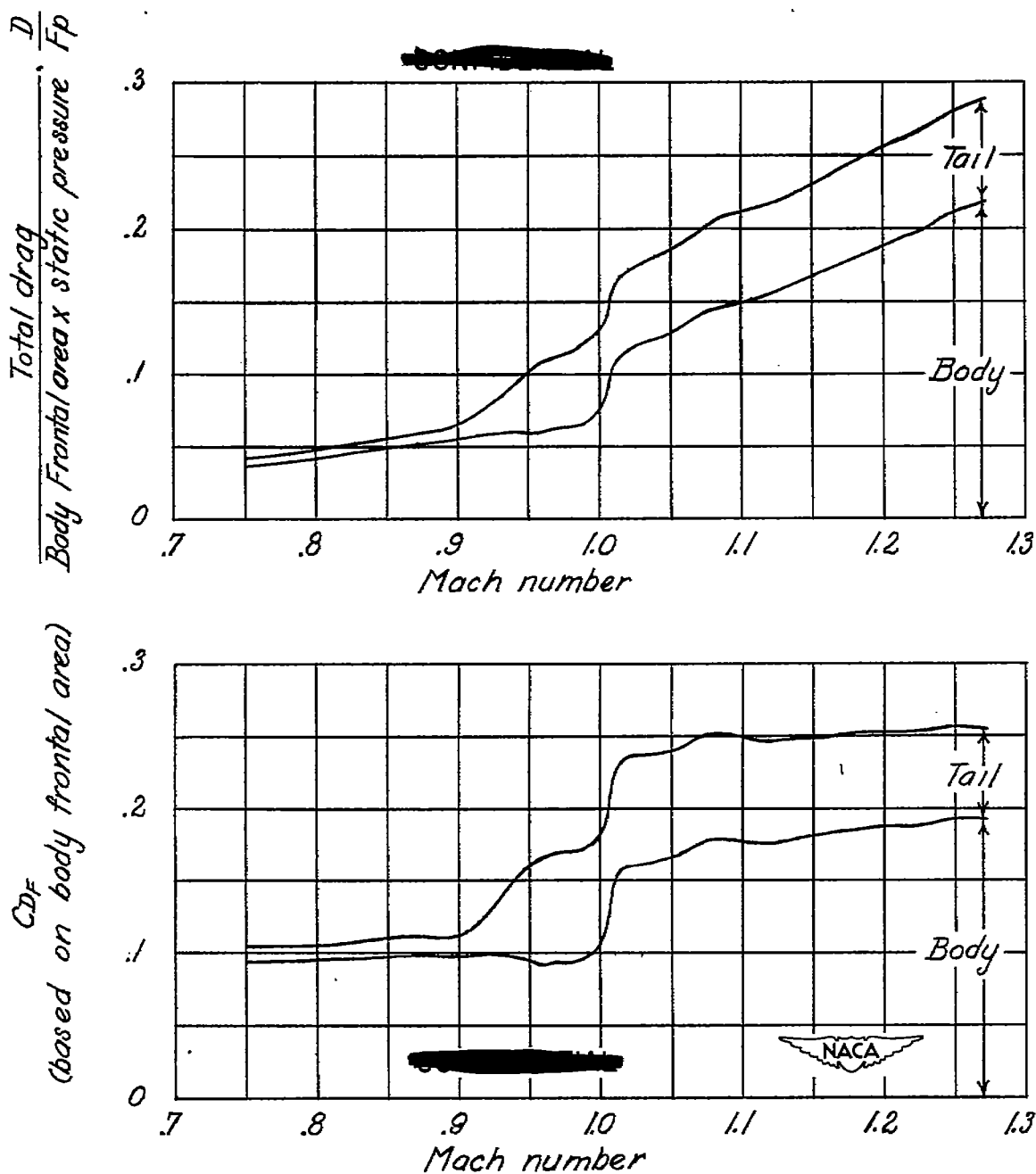
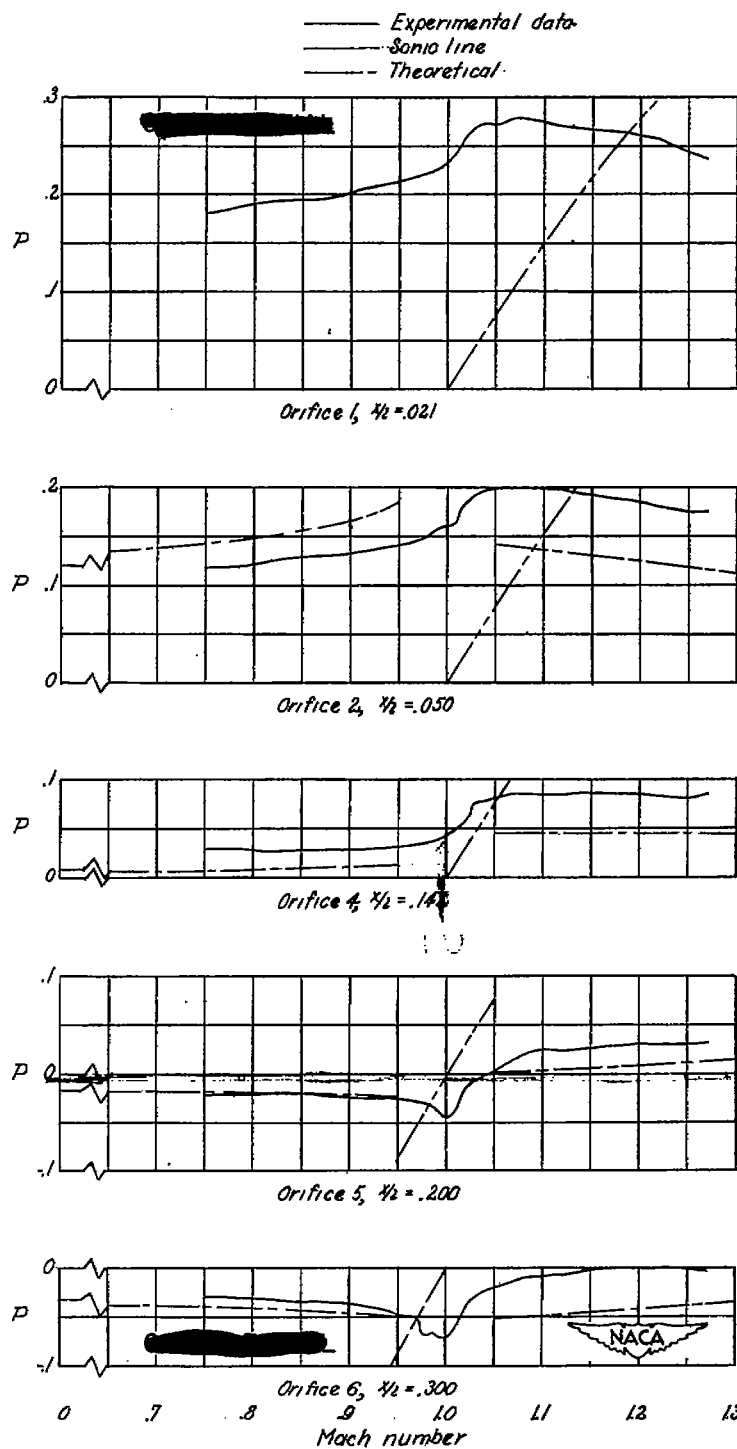
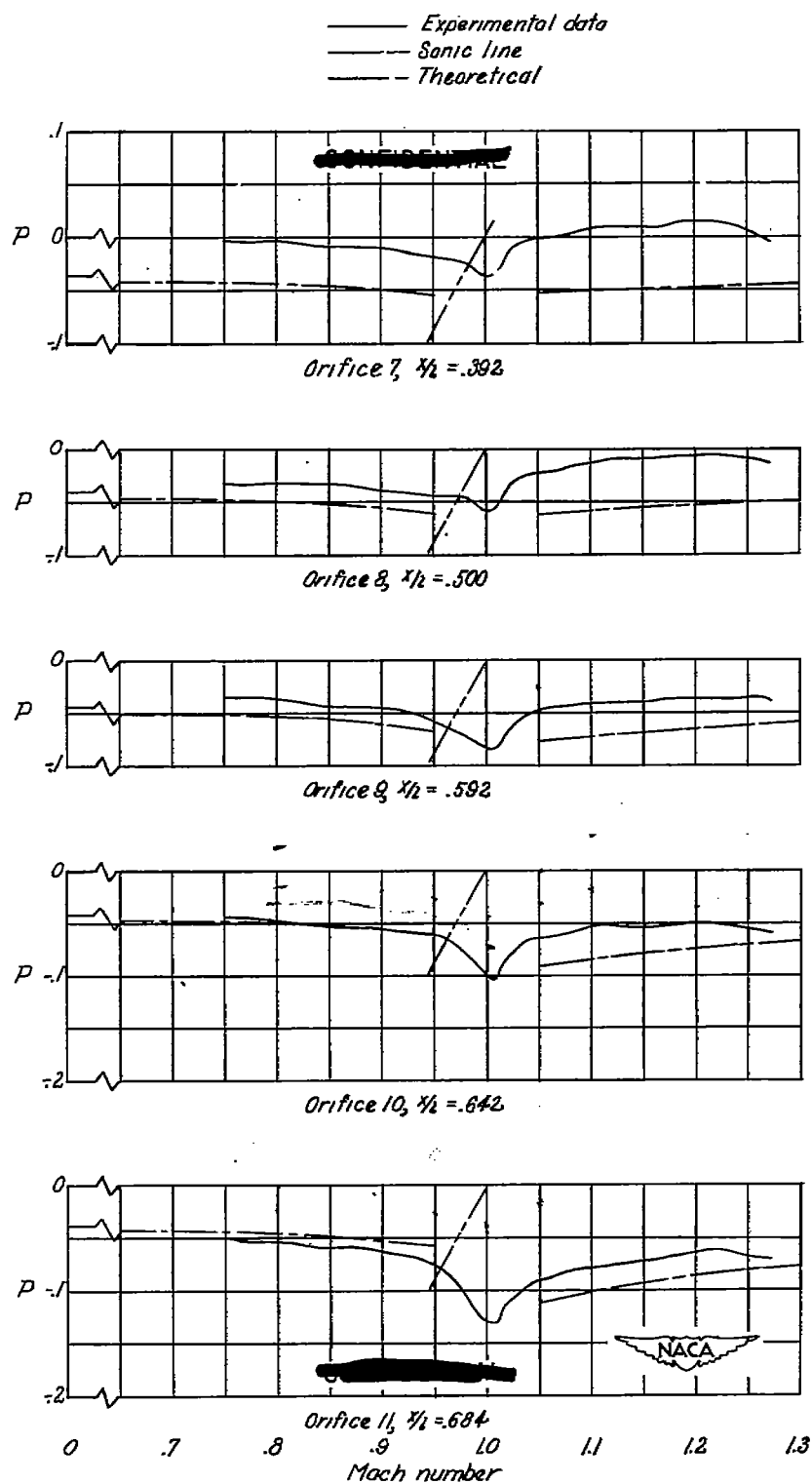


Figure 3.- Variation with Mach number of D/F_p and C_{D_F} for the complete model and its component parts as obtained from the accelerometer and tail-drag measurements.



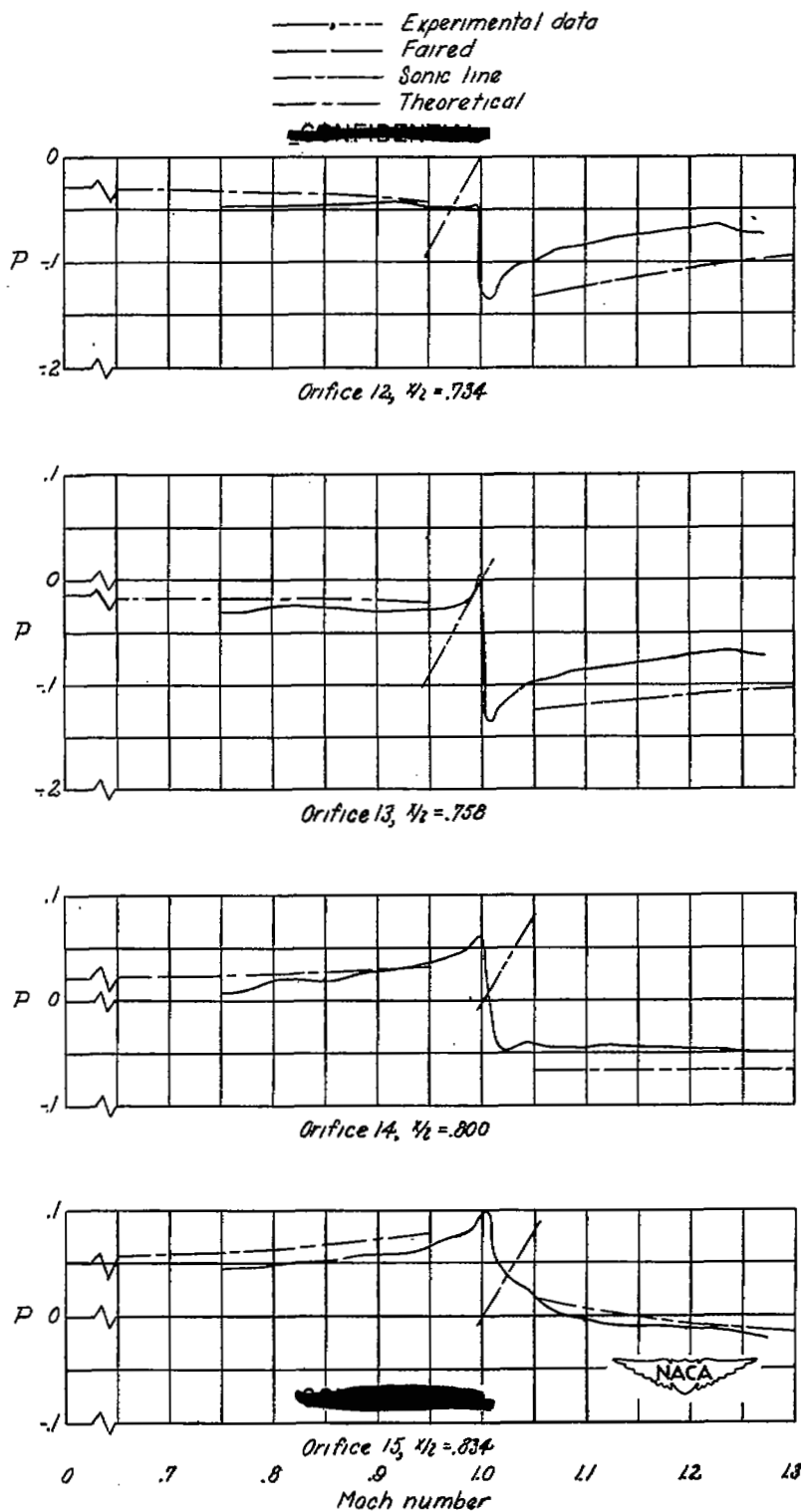
(a) Orifices 1 to 6.

Figure 4.- The variation with Mach number of the pressure coefficient P for each orifice and comparison with theoretical variations computed by the method of reference 5 at subsonic speeds and reference 1 at supersonic speeds.



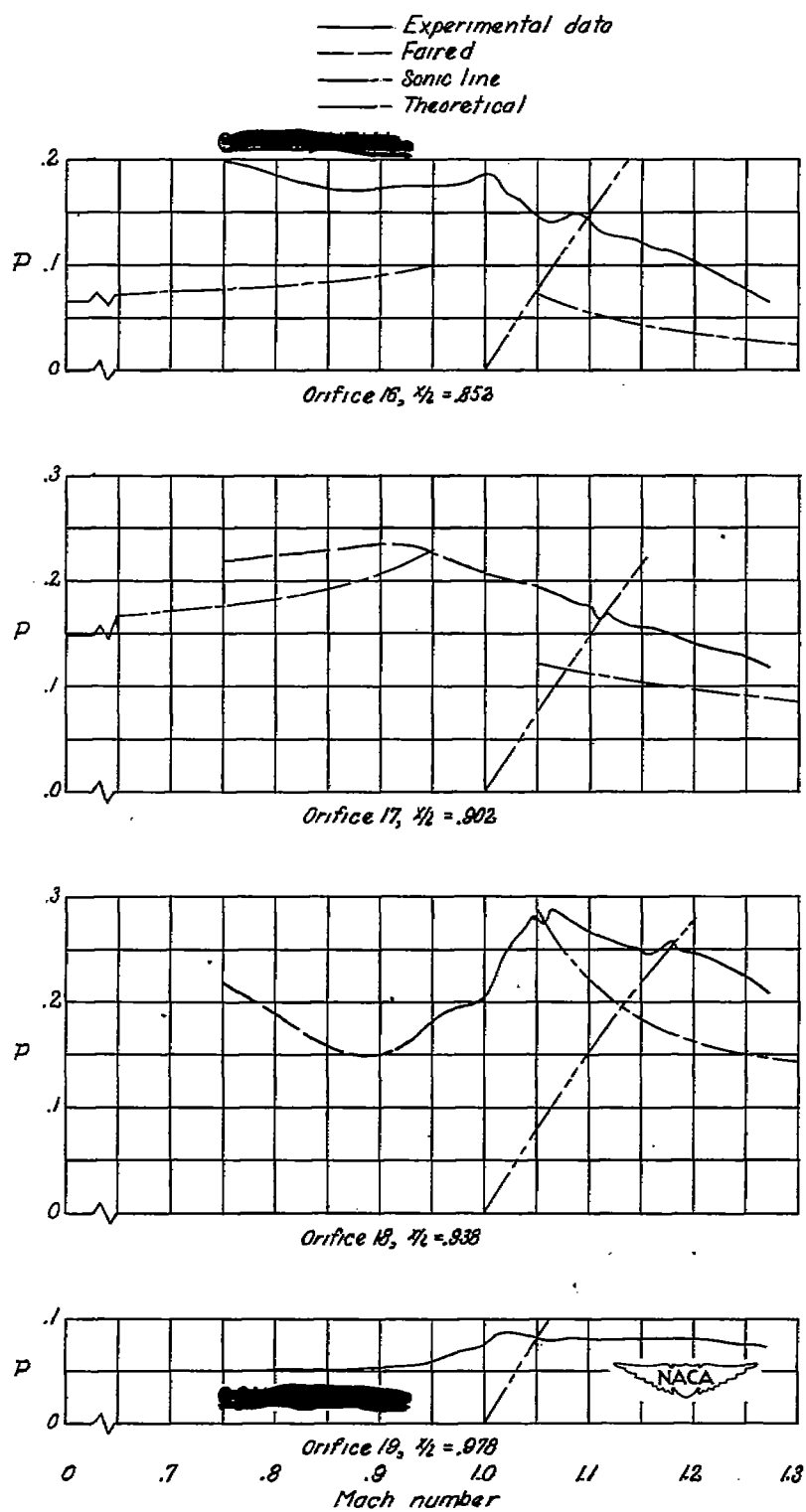
(b) Orifices 7 to 11.

Figure 4.- Continued.



(c) Orifices 12 to 15.

Figure 4.- Continued.



(d) Orifices 16 to 19.

Figure 4.- Concluded.

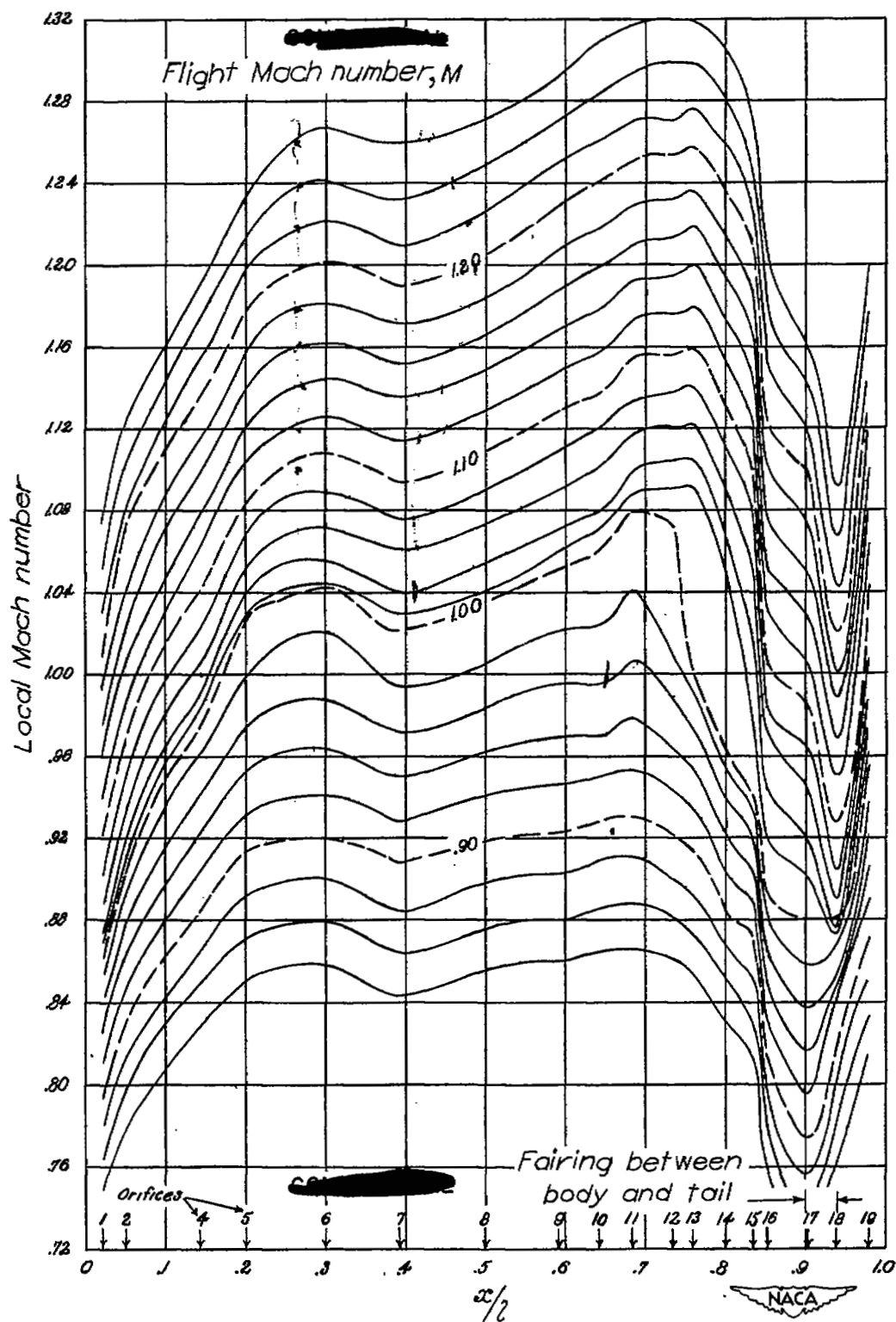


Figure 5.- The variation with position along the body x/l of the local Mach number for even values of free-stream Mach number. The orifice locations are shown at the lower edge of the figure.

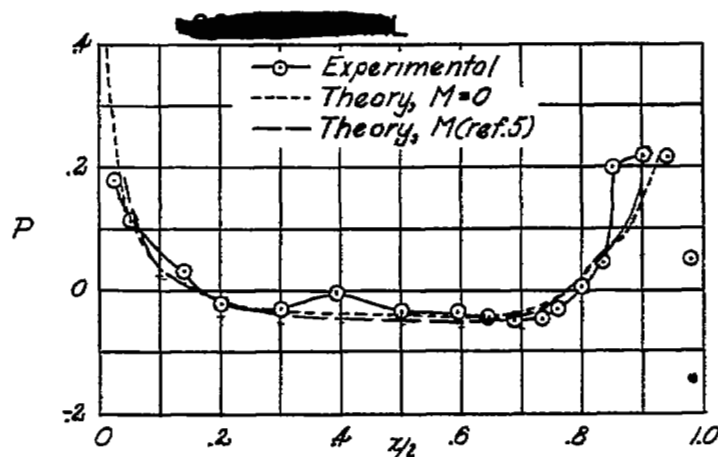
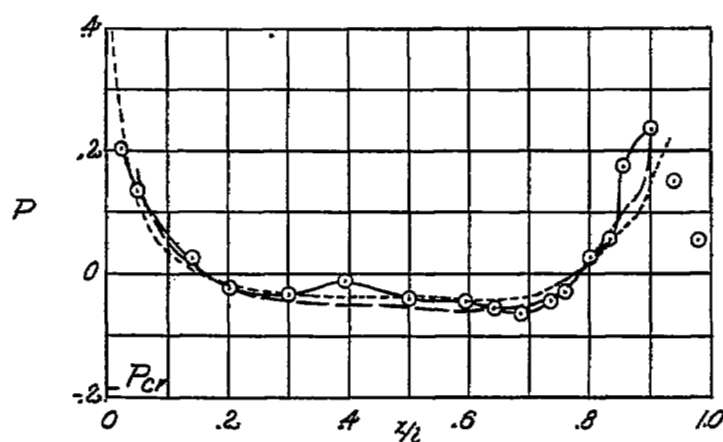
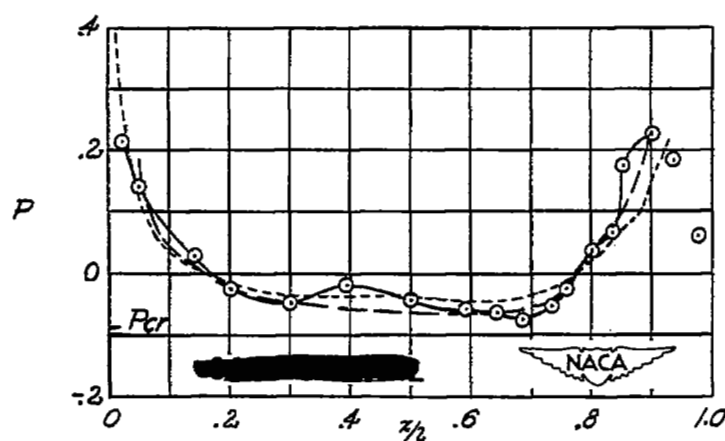
(a) $M = 0.75$.(b) $M = 0.90$.(c) $M = 0.95$.

Figure 6.- Variation of pressure coefficient P with position along the body x/l for several Mach numbers. The experimental measurements are compared with theoretical pressure distributions computed for the subject body and with the value of P corresponding to local sonic velocity, P_{cr} .

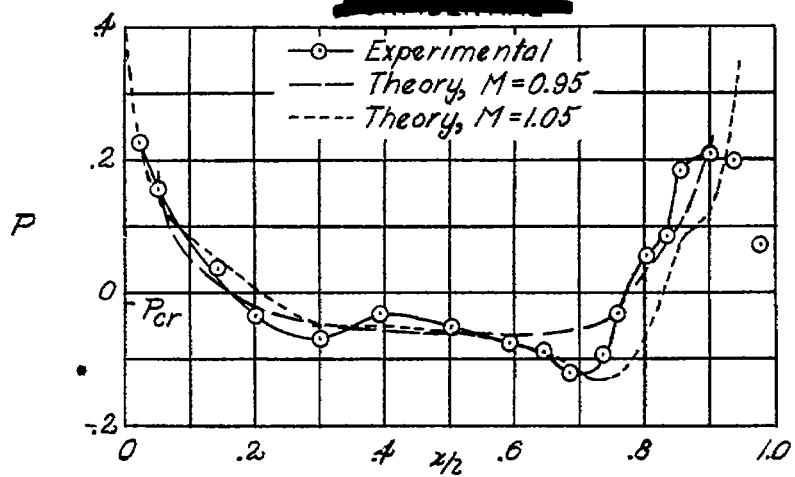
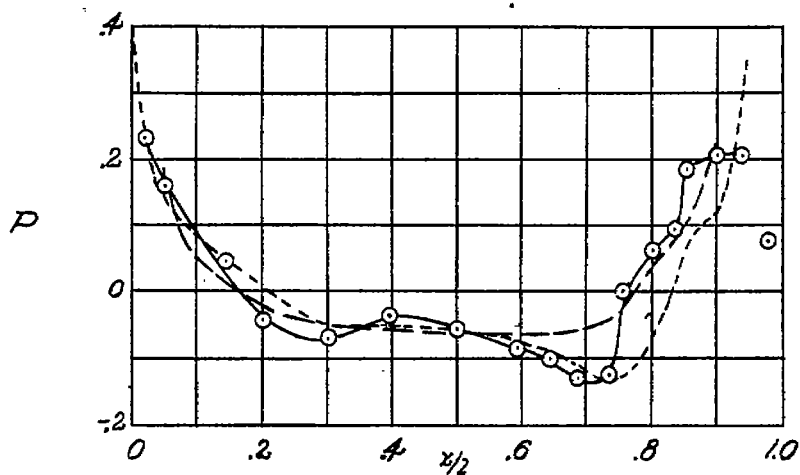
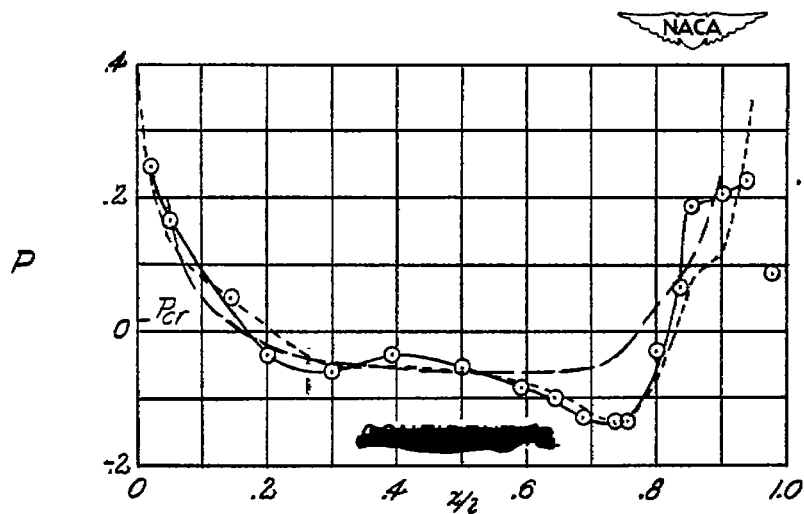
(d) $M = 0.99$.(e) $M = 1.00$.(f) $M = 1.01$.

Figure 6.- Continued.

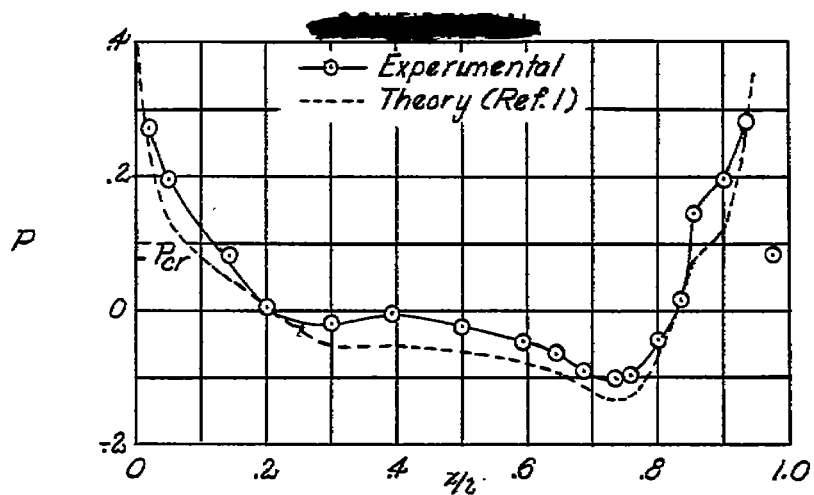
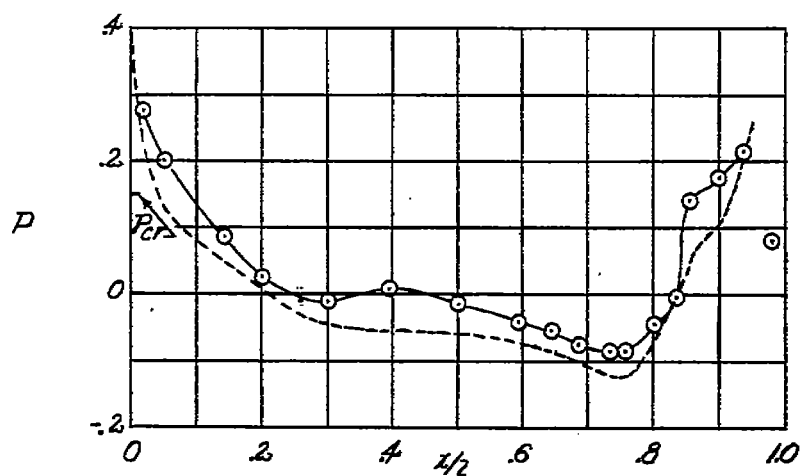
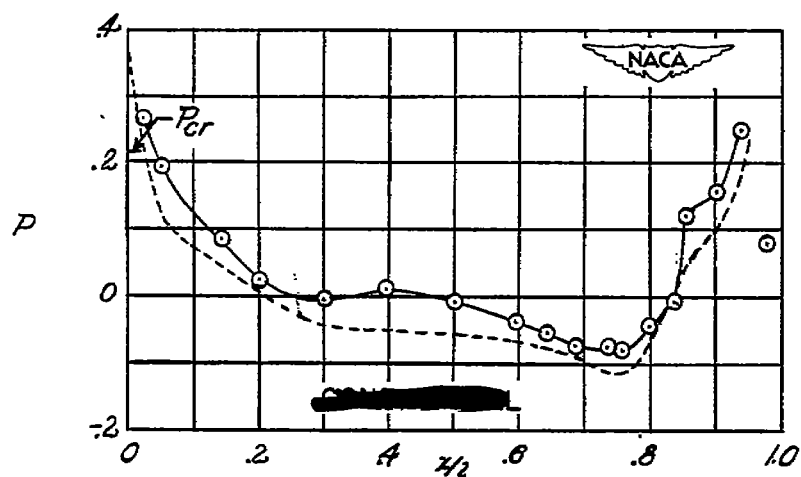
(g) $M = 1.05$.(h) $M = 1.10$.(i) $M = 1.15$.

Figure 6.- Continued.

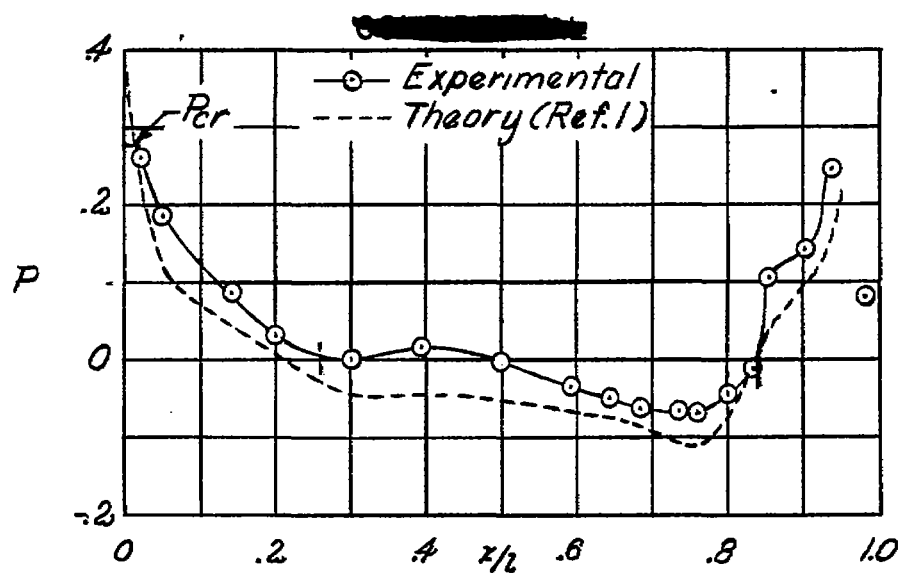
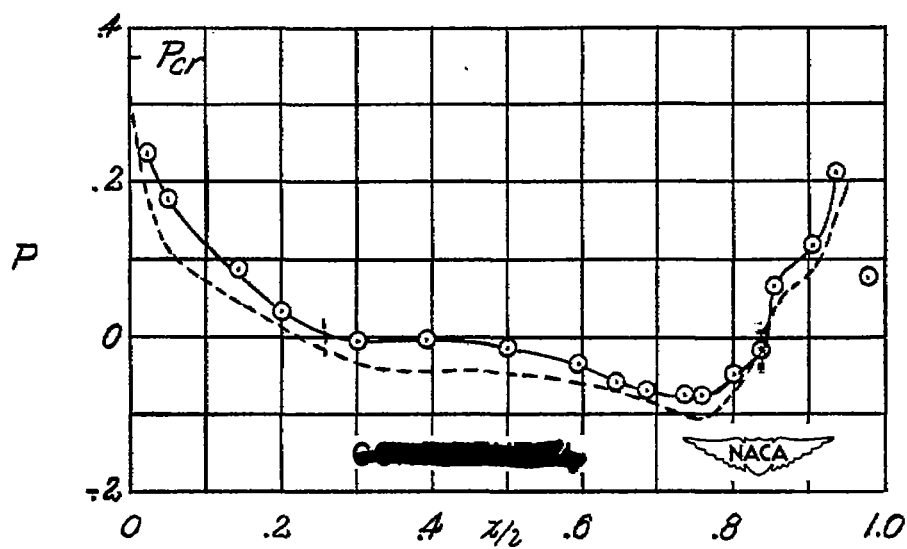
(j) $M = 1.20$.(k) $M = 1.27$.

Figure 6.- Concluded.

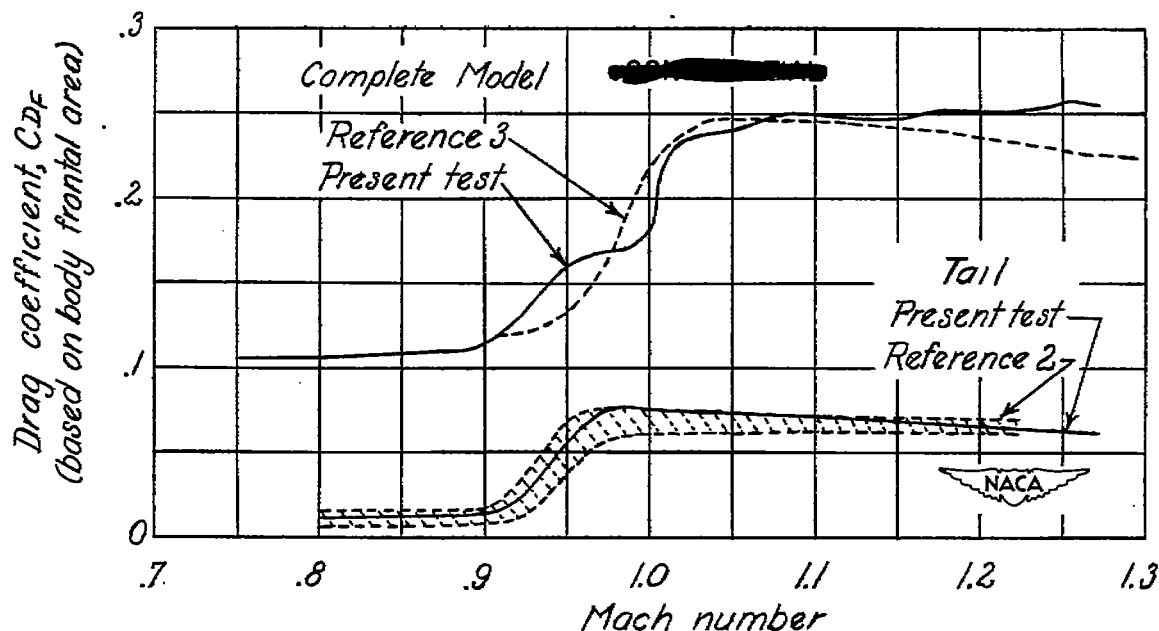


Figure 7.- Comparison with previous results of the measured variation of drag coefficient with Mach number for the complete model and for the tail of the subject model.

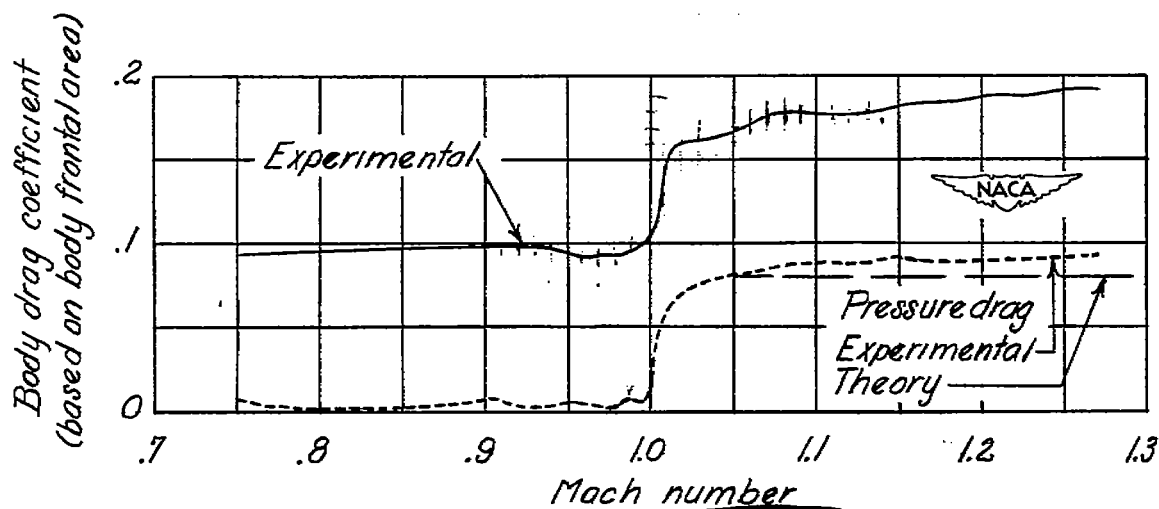


Figure 8.- Variation with Mach number of body drag coefficient determined from data of figure 7 and of the body pressure-drag coefficient. Pressure drag at supersonic speeds computed from reference 1 is included for comparison.

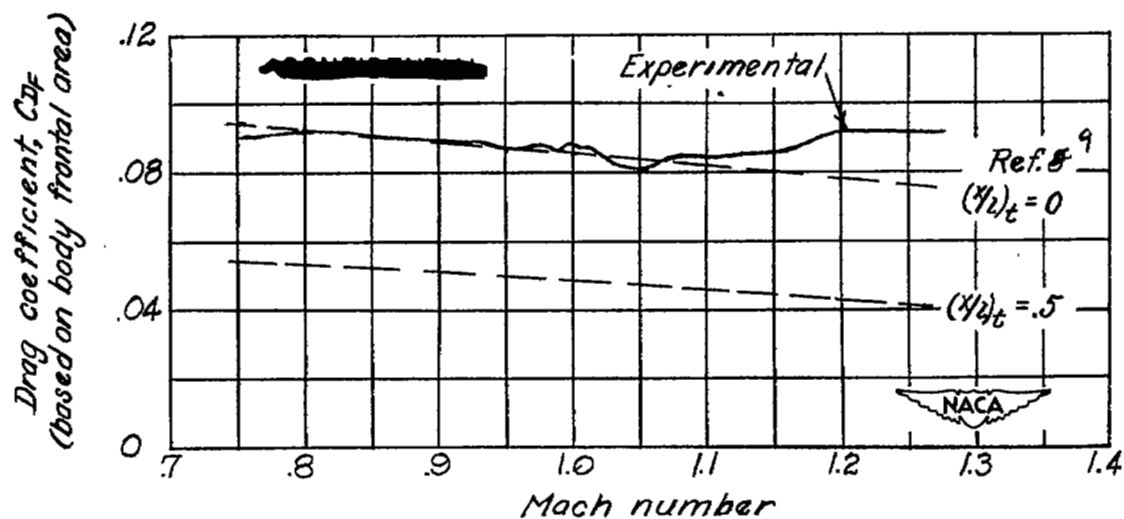


Figure 9.- Comparison of skin-friction drag coefficient determined from data of figure 8 and comparison with theory.

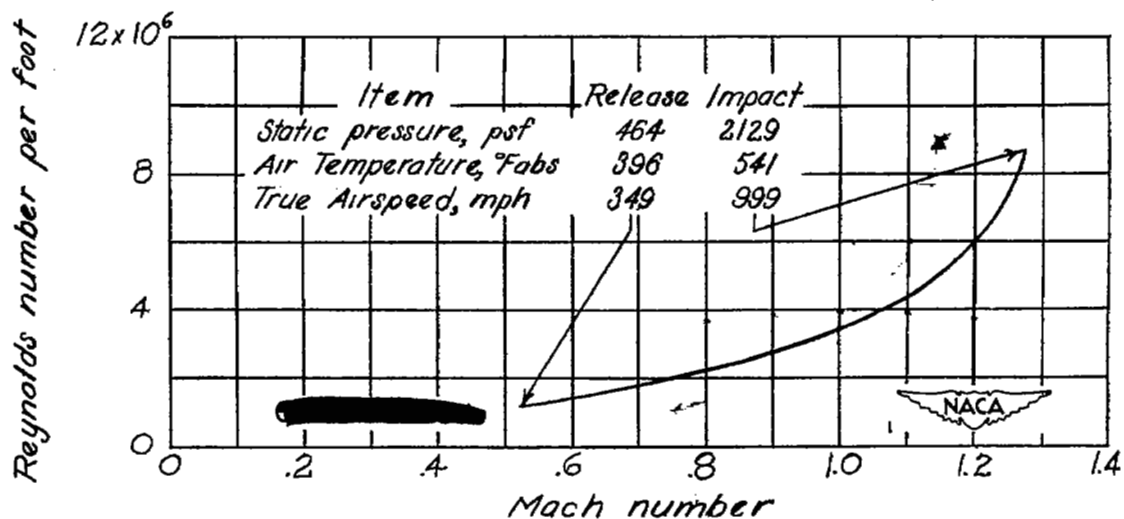


Figure 10.- Variation of Reynolds number per foot with Mach number during the subject test. Conditions at the beginning and end of the free fall are included.